



# Recent Advances in Positron Emission Tomography/Magnetic Resonance Imaging Technology

Hossein Arabi, PhD<sup>a</sup>, Habib Zaidi, PhD<sup>a,b,c,d,\*</sup>

## KEYWORDS

- PET/MRI • Multimodality imaging • Instrumentation • Quantitative imaging • Attenuation correction

## KEY POINTS

- Contrary to the widespread adoption of hybrid PET/CT scanners in clinical setting, PET/MR imaging bears only a small fraction of the total PET market.
- PET/MR imaging is challenged by MRI-guided attenuation correction of PET data, mutual MR-PET components interferences, body truncation, and metal artifacts.
- The trend is toward developing compact PET inserts for existing MRI scanners, providing high spatial resolution and reasonable cost.
- Deep learning-guided approaches will be predominately employed to address the major challenges of quantitative PET/MR imaging.

## INTRODUCTION

Over a decade has passed since the introduction of PET/MR hybrid systems in the clinic, wherein the main advantages and drawbacks of PET/MR imaging from a medical, technical, and logistics/workflow perspective have been investigated.<sup>1,2</sup> In contrast to the widespread adoption of hybrid PET/CT scanners in the clinical setting, PET/MR imaging couldn't reach many sites and may bear only 5% of the total PET market.<sup>3</sup> This trend could be attributed to the high cost and new paradigms introduced by this technology, workflow, and logistics issues, and the challenges associated with quantitative PET/MR imaging. Since the introduction of PET/MRI systems, substantial efforts have been made to find/establish the key clinical applications of this modality in order to justify/promote its utilization.

Though PET/MR systems are not as popular as PET/CT scanners, they cause reduced patient radiation exposure, which is critical in childbearing women, pediatric patients, and patients undergoing sequential response to therapy and recurrence monitoring.<sup>4,5</sup> Moreover, superior soft-tissue contrast and visualization in MR images (compared to CT images) would lead to enhanced lesion detectability and diagnostic accuracy in addition to complementary functional information that could be provided by MR imaging.<sup>6,7</sup> Furthermore, simultaneous PET and MR imaging would enable motion correction to PET data to compensate for respiratory and cardiac motions as well as patient movement due to pain and anxiety during PET imaging.<sup>8</sup> Reduced positron range and improved PET image quality (higher spatial resolution) are expected for high-energy positron-emitting PET radiotracers due to the presence of the MR magnetic

<sup>a</sup> Division of Nuclear Medicine and Molecular Imaging, Geneva University Hospital, Geneva 4 CH-1211, Switzerland; <sup>b</sup> Geneva University Neurocenter, Geneva University, Geneva CH-1205, Switzerland;

<sup>c</sup> Department of Nuclear Medicine and Molecular Imaging, University of Groningen, University Medical Center Groningen, Groningen 9700 RB, Netherlands; <sup>d</sup> Department of Nuclear Medicine, University of Southern Denmark, Odense 500, Denmark

\* Corresponding author. Division of Nuclear Medicine and Molecular Imaging, Geneva University Hospital, Geneva 4 CH-1211, Switzerland.

E-mail address: habib.zaidi@hcuge.ch

field in simultaneous PET MR imaging at high magnetic field strength.<sup>9</sup> Moreover, co-registered MR data (in simultaneous PET/MR imaging) could be employed for MRI-guided PET image reconstruction and partial volume correction to enhance the overall quality and quantitative accuracy of PET images.<sup>10,11</sup>

Despite the advantages associated with simultaneous PET/MR imaging, this technology yet faces major challenges regarding attenuation correction for PET data, mutual MR-PET components interferences, body truncation due to the limited transaxial MR field-of-view, and artifacts in MR images due to the metal implants.<sup>12</sup>

In this review, the latest technical developments in PET/MR systems design and technological developments as well as the state-of-the-art solutions to the major challenges of quantitative PET/MR imaging are discussed.

### ADVANCES IN POSITRON EMISSION TOMOGRAPHY/MAGNETIC RESONANCE IMAGING INSTRUMENTATION

The major challenge to developing simultaneous PET/MR devices is to minimize/nullify the interference between the magnetic field of MR imaging and the readout electronics of PET detectors.<sup>13</sup> In this regard, PET photomultiplier tubes (PMT) were replaced by semiconductor components in PET detectors. The very first simultaneous PET/MRI system (for small-animal imaging) exploited avalanche photodiodes (APD) coupled to lutetium oxyorthosilicate (LSO) crystals in a 7T MR scanner.<sup>14,15</sup> Using the same technology, Siemens Healthcare (Erlangen, Germany) built a prototype PET insert for simultaneous brain imaging in a 3T MR scanner with a 36 cm inner diameter.<sup>16</sup> PET detectors were shielded in copper cassettes to minimize magnetic field interferences. No noticeable interferences were reported between PET and MR components, such as PET signal distortion, eddy currents in PET shields, and inhomogeneities of the magnetic field (B0).<sup>17</sup>

The first whole-body PET/MR scanner (Ingenuity TF PET/MRI) was installed by Philips Healthcare in 2010. To avoid the interferences between PET and MR components, sequential hybrid imaging was adopted in this scanner, wherein the time of flight (TOF)-PET component of the Philips Gemini PET/CT was combined with Philips Achieva 3T MRI scanner (using a turntable-based mechanism). Owing to the sequential acquisition, no novel instrumental development was considered in the PET component, and still, PMTs (together with LYSO crystals) were employed in the PET detectors with minor modifications.<sup>18,19</sup> The Biograph mMR

(hybrid whole-body PET/MR, Siemens) was the first commercial whole-body scanner allowing for simultaneous MR imaging and PET data acquisition.<sup>20</sup> To reduce the sensitivity of the PET detectors to the 3T magnetic field, APDs were employed as readout electronics of photon detectors (LSO) with a crystal size of  $4 \times 4 \times 20$  mm<sup>3</sup>, leading to a spatial resolution of 4.3 mm (FWHM). Due to the slower temporal performance of APDs compared to PMTs, the PET device does not benefit from TOF capability. Even though the PET component was fully integrated within the MR scanner, no significant distortion was observed in the RF field (B1) and magnetic field (B0) homogeneity as well as interferences of MR signals with the PET electronics.<sup>20</sup> 4-channels coils were later introduced in this system for dedicated MR imaging (breast scans) which caused 11% reduction in the PET statistical counts (photon attenuation).<sup>21</sup> Simultaneous PET and MR (3T) imaging SIGNA system was introduced by GE Healthcare in 2014 using Lutetium-based scintillator (LBS) crystal and Light Tight RF Shield with copper coating. The PMTs or APDs were replaced with Silicon Photomultipliers (SiPMs) in this scanner providing a similar gain of  $10^6$  for PMTs (compared to  $10^2$  provided by APDs) and 400 ps temporal resolution compared to 1 ns for PMTs.<sup>22</sup> These commercial PET/MR scanners have a large MR bore size of 70 cm to accommodate the PET component, however, the bore size of PET devices would be 60 cm in diameter, which may cause claustrophobia issues and limit the choice of subjects in terms of body size. The most recently released simultaneous uPMR790 PET/MRI scanner (United Imaging Healthcare Co. Ltd., Shanghai, China) has shown reliable performance with its 60 cm transverse field-of-view (FOV) of and 32 cm FOV.<sup>23</sup>

APDs are highly sensitive photodiodes that convert light into electricity based on the photoelectric effect. In the early PET/MR systems, APDs gained popularity owing to their very low sensitivity to the magnetic field, though they provide remarkably lower amplification gain compared to PMTs ( $10^2$  vs  $10^6$ ).<sup>24</sup> SiPMs addressed the shortcomings of APDs through providing similar amplification gains to PMTs while requiring a low supply voltage (eg, 40 v vs 400 v for APDs). SiPMs are the dominant photodetectors in PET technology, however, the trend is toward using fully digital SiPMs wherein the photons are counted/detected in a digital format which renders the sensor less susceptible to electronic noise, magnetic field interferences, and temperature variations.<sup>25</sup>

Owing to the efficient performance of SiPMs in strong magnetic fields, brain PET inserts gained momentum and were designed and built for 7T

MR imaging using this technology. In this regard, Cubresa BrainPET, a PET insert for MR scanners (compatible with major MR scanners), was designed to provide simultaneous PET and 3T MR imaging capability comparable or superior to commercial competitors.<sup>26</sup> As a PET insert, the Cubresa BrainPET is conveniently lifted and mounted on the bed of MR scanners. The BrainPET technology relies on the preclinical Cubresa NuPET family (animal PET inserts for 7T MR scanners) with LYSO detectors coupled to SiPM modules.<sup>27</sup> The Cubresa NuPET inserts are compatible with commercial MR scanners operating at 1.5 to 9.4 T MR field strengths.<sup>28</sup> The Cubresa NuPET inserts (different versions) provide transaxial FOV of 59 mm to 250 mm and spatial resolution of 0.9 mm to 1.7 mm.<sup>28</sup> The major PET performance parameters, such as spatial resolution, SNR, and quantitative accuracy were altered when PET inserts were operating at 7T magnetic field, while MR parameters (Bruker 7T MRI scanner, Biospin, Billerica, MA) were not affected by the presence of the PET inserts.<sup>28,29</sup>

The MINDView PET brain imager was designed to function as an insert into 3T mMR scanner benefiting from monolithic LYSO detectors. The effective FOV of the scanner is 24 cm in diameter and 15.4 cm in axially. This PET scanner provided spatial resolution of less than 2 mm and exhibited no remarkable performance deviation when MR sequences such as MPAGE and ultrashort time echo were simultaneously acquired.<sup>30</sup>

To perform brain PET scanning in a single bed position, a brain PET insert based on LSO and SiPM modules was designed and built for the 7T Magnetom (Siemens Healthineers) MRI scanner.<sup>31</sup> This PET insert is equipped with depth of interaction (DOI) capability and provides axial and transaxial FOVs of 16.7 and 25.6 cm, respectively. Though this scanner offers a peak sensitivity of 18.9 kcps/MBq and a spatial resolution of 2.5 mm (according to the NEMA NU 2 standard), its performance within simultaneous MR imaging should be improved. Fig. 1 depicts this brain PET insert prototype together with PET images of the hot-rod and 3D Hoffman phantoms.

In an effort to build a flexible PET scanner to be attached/linked to existing MR scanners, fxPET scanner was developed using a dual arc-shape spinning detector covering 135°. The ring diameter and axial extent of this scanner are 77 and 15 cm, respectively, which enables whole-body sequential PET/MR imaging.<sup>32</sup> In the context of simultaneous data acquisition, the approach adopted by the TRIMAGE consortium should be considered, where simultaneous electroencephalography (EEG)/PET/MR scans are performed for a comprehensive

study of basic mechanisms in the brain.<sup>33</sup> The PET component has an inner diameter and axial FOV of 26 and 16 cm, respectively, inserted into a 1.5 T MR scanner.

## PRECLINICAL POSITRON EMISSION TOMOGRAPHY/MAGNETIC RESONANCE IMAGING SYSTEMS

The majority of preclinical PET/MRI scanners employ LYSO crystals readout by SiPMs owing to their high resolution and compact design. One such example is the hybrid SimPET scanner (Brightonix Imaging Inc., Seoul, South Korea). This PET/MR scanner benefits from a permanent 1T magnet and a PET ring which is capable to work within a 7T magnetic field with an inner bore diameter of 6.0 cm. SimPET-X PET insert was later introduced for total-body mouse PET/MR scanning (using LSO crystals) with 11 cm axial FOV and remarkably superior sensitivity compared to SimPET.<sup>34</sup>

Bruker BioSpin (Ettlingen, Germany), as one of the major vendors in the preclinical field, offered a dedicated PET insert to operate in a 9.4 T magnetic field followed by the release of a sequential PET system for MR scanners up to 15.2 T.<sup>35</sup> NuPET (Cubresa, Winnipeg, MB, Canada) and HALO (Inviscan Imaging Systems, Strasbourg, France) PET inserts were designed to fit into most commercially available MR scanners. Mediso Medical Imaging Systems (Budapest, Hungary) and MR Solutions (Guildford, Surrey, United Kingdom) companies produced preclinical PET/MR and PET inserts which could operate in stand-alone or sequential modes.<sup>36</sup>

SAFIR-I, a preclinical PET insert for 7T MRI scanners, was built for high-rate kinetic examination of rats and mice using injected activity up to 500 MBq. This scanner, with an axial FOV of 54.2 mm and an inner diameter of 114 mm, allows for time frames of a few seconds with an acceptable signal-to-noise ratio and spatial resolution of about 2 mm (at the center of the FOV).<sup>37</sup> Representative PET images of the rat brain obtained from the SAFIR-I PET scanner at 5 s time frame are presented in Fig. 2.

A recent survey on the Cubresa NuPET insert (Cubresa, Inc., Winnipeg, MB) inserted in a Bruker 7T MRI scanner (Bruker Biospin, Billerica, MA) revealed that some key characteristics of PET imaging, such as quantitative accuracy, signal-to-noise ratio (SNR), and spatial resolution, as well as MRI SNR, were adversely affected in the presence of both PET and MR components.<sup>28</sup> PET images of the Derenzo phantom filled with <sup>18</sup>F-FDG and <sup>68</sup>Ga are shown in Fig. 3 when the PET

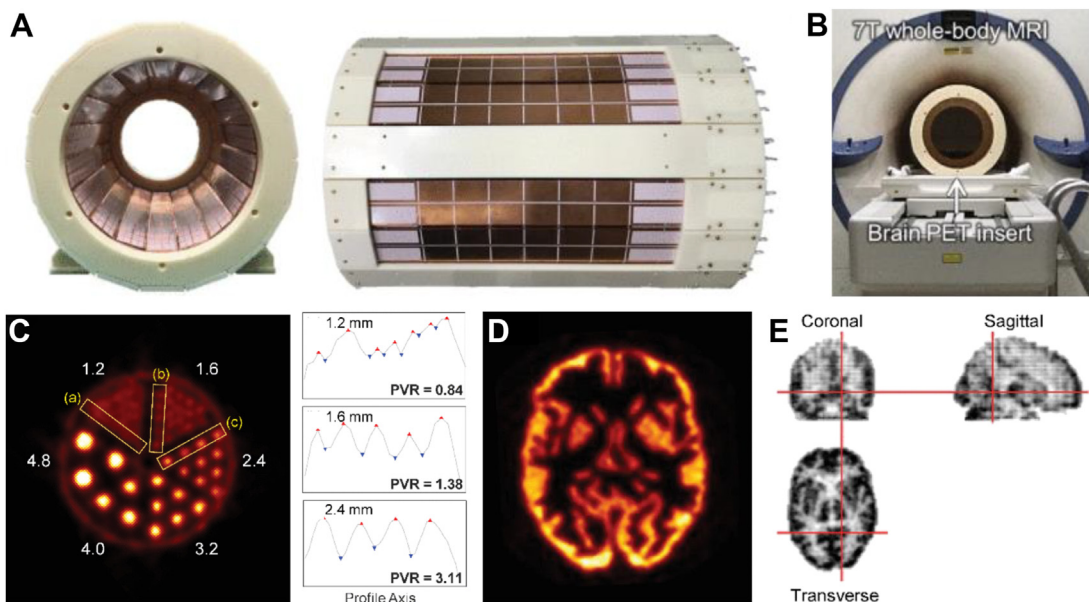


**Fig. 1.** (A) Prototype brain PET insert built by Won and colleagues,<sup>31</sup> (B) Brain PET scanner inserted in a 7T MR scanner, (C) PET image of the hot-rod phantom along with line profiles through the 1.2 mm, 1.6 mm, and 2.4 mm hot rods. PVR refers to the peak valley ratio. (D) PET image of 3D Hoffman brain phantom. (Adapted with permission from<sup>31</sup> under a Creative Commons License.)

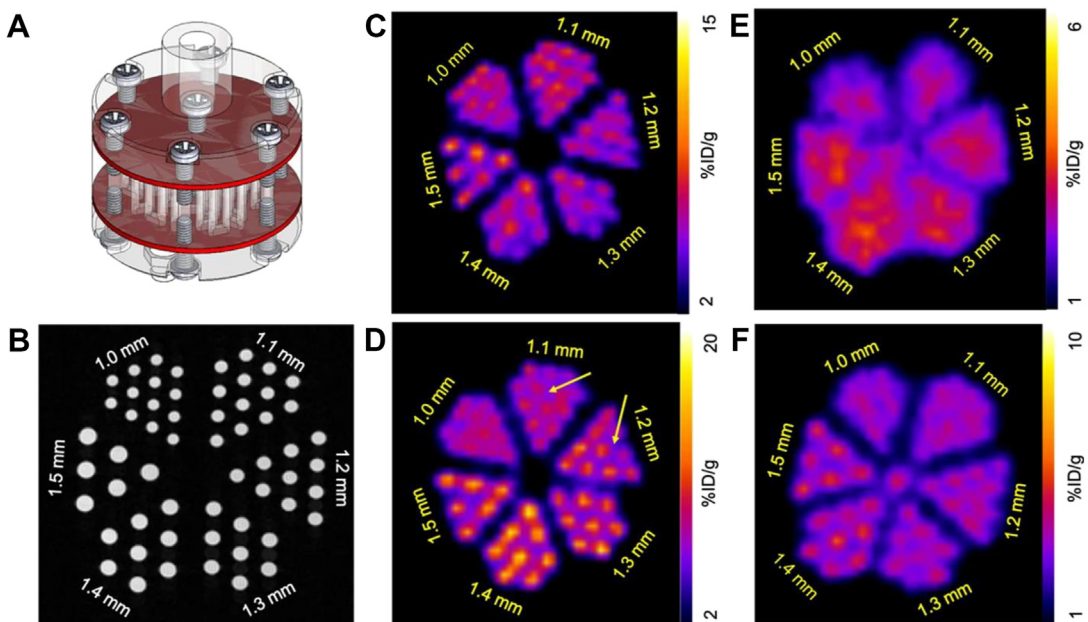


**Fig. 2.** (A) The Derenzo phantom, (B) MR images, (C) PET image of the phantom with 3.7 MBq of  $^{18}\text{F}$ -FDG at the center of the FOV, (D) PET image of the phantom when the PET component<sup>28</sup> was inserted into the MRI scanner, (E) PET image of the phantom with 3.7 MBq  $^{68}\text{Ga}$  at the center of the FOV, and (F) PET image of the phantom (with  $^{68}\text{Ga}$ ) when the PET component was inserted into the MRI scanner. (Reprinted with permission from Springer Nature<sup>28</sup> under a Creative Commons License.)

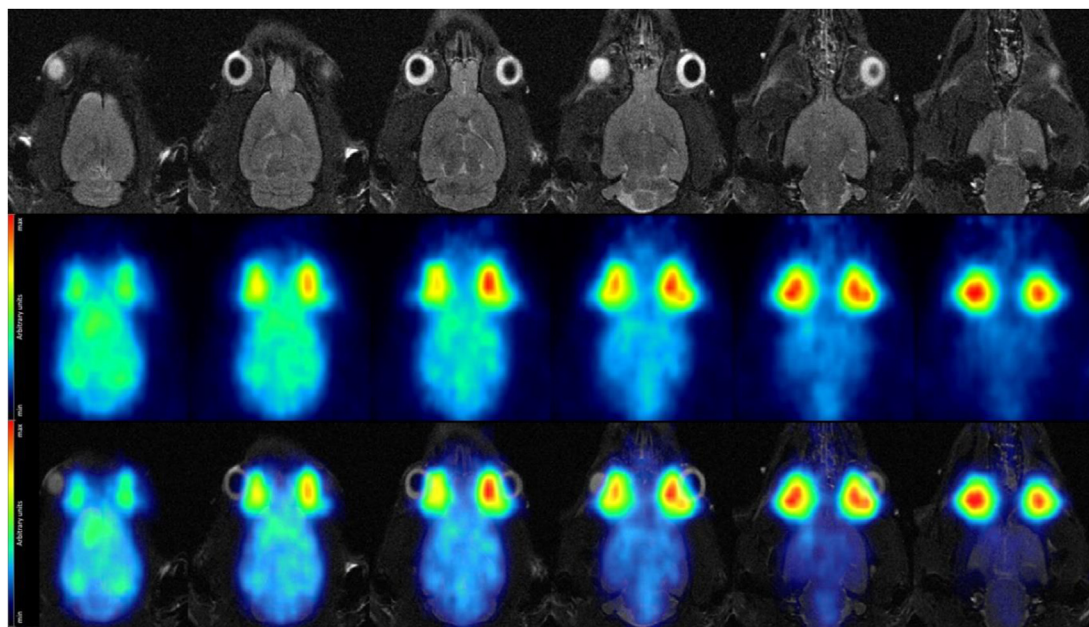


**Fig. 3.** (Top row) MR images (coronal views) of a rat brain obtained with a T2-TurboRARE sequence, (Middle row), Corresponding PET images at high activity ( $>300$  MBq) in a single 5-s time frame, (Bottom row) Fused PET and MR images acquired on the scanner described in.<sup>37</sup> (Reprinted from<sup>37</sup> under a Creative Commons License.)

component was outside and within the MRI scanner. A similar study on the MR Solutions PET insert (model I-402, Guildford, UK) installed in a 3T MRI scanner demonstrated no significant interference between PET and MR components when they were operating in a stand-alone or simultaneous PET and MR acquisition mode.<sup>38</sup>

#### PROGRESS IN MAGNETIC RESONANCE IMAGING-GUIDED ATTENUATION CORRECTION IN HYBRID POSITRON EMISSION TOMOGRAPHY/MAGNETIC RESONANCE IMAGING

The major challenge impacting quantitative PET/MR imaging is the correction for attenuated photons within the body and other devices in the PET FOV. Since MR signals indicate tissue proton density and relaxation times and are not correlated with electron density, photon attenuation coefficients of materials cannot be directly estimated from MR images.<sup>39</sup> In addition to estimating linear attenuation coefficients from MR signals, quantitative PET/MR imaging faces the challenges of image artifacts due to metallic implants, body truncation in MRI-derived attenuation correction maps (AC maps), MRI hardware inside the PET FOV, and mismatches between MR and PET images.<sup>40</sup> A number of reports demonstrated that MRI Gadolinium-based contrast agents do not have a significant impact on PET quantification.<sup>41</sup>

In early PET/MRI systems, simple segmentation/classification of major tissue classes from T1-weighted and Dixon MR sequences was conducted to generate AC maps for PET data.<sup>18,42</sup> Due to the extremely short T1 relaxation time of cortical bone, bony structures were missing in the segmentation-based AC maps and they only included air, lung, soft-tissue, and fat tissue types.<sup>43,44</sup> The omission of bony structures from PET AC maps led to noticeable bias in the estimation of tracer uptake within/close to bones.<sup>45</sup> To address this issue, ultra-short, and zero echo time sequences were employed for bone visualization and inclusion in MRI-derived PET AC maps.<sup>46,47</sup> However, due to long acquisition times and misclassification of adjacent bone and air, these sequences were not feasible in head and neck imaging.<sup>48</sup>

An alternative approach to include bony structures in MRI-derived AC maps is to employ an off-line bone template (consisting of major bone structures such as skull, hip, femur, and spine) that is to be aligned/registered to the MR image of the patient (referred to as atlas-based methods).<sup>49</sup> The SIGNA (GE Healthcare) and mMR (Siemens Healthineers) hybrid PET/MR scanners are equipped with short echo time MR sequences or atlas-based methods to include bony structures in brain AC maps.<sup>43</sup> Mixed feedback was received from the clinical implementation of the atlas-based method concerning inaccurate bone alignment and gross misregistration errors.<sup>50</sup>

Anatomic abnormalities would not be taken into account in atlas-based approaches, thus leading to remarkable patient-wise errors.<sup>51</sup> With respect to the fact that raw PET data inherently bear information about both emission and attenuation, maximum likelihood attention and activity reconstruction (MLAA) approaches could be employed to generate patient-specific PET AC maps and/or PET attenuation-corrected images.<sup>52</sup> Though this approach suffers from high levels of noise and uncertainties in the estimation of the attenuation coefficients, the quantitative errors due to metallic implants (metal artifacts) and body truncation could be diminished by this approach.<sup>53,54</sup>

The remarkable performance of convolutional neural networks is about to bring a paradigm shift in multimodality medical imaging, including PET/MRI technology.<sup>55,56</sup> Promising results have been achieved using deep learning approaches in synthetic CT generation or PET map estimation from MR images which closely follow CT-based AC maps.<sup>57</sup> Moreover, deep learning approaches have enabled novel approaches to address the challenge of AC in PET/MRI imaging such as directly applying attenuation and scatter correction on non-AC PET images in the image domain,<sup>58</sup> estimation of attenuation correction factors in the sinogram domain,<sup>59</sup> estimation of accurate PET AC maps from the outcome of MLAA approaches,<sup>60</sup> and synthetic CT generation from non-AC PET images.<sup>61</sup> Overall, these approaches have reported quantitative bias of less than 10% for the recovery of activity concentration compared to ground truth CT-based AC of PET data, which is considered as clinically tolerable errors. A comparison of segmentation-based, atlas-based, and deep learning-based synthetic CT generation from MR images are depicted in Fig. 4.

### **Hardware-based Attenuation Correction**

In addition to photon attenuation within the patient's body, MR equipments (eg, MR coils, patient positioning devices, and so forth) inside the PET FOV cause significant photon attenuation which should be taken into account for quantitative PET imaging.<sup>62</sup> Rigid MR hardware could be easily modeled within PET image reconstruction using a predetermined attenuation map. However, flexible MR hardware (eg, carotid coils and headphones) require localization, including markers, ultra-short echo time sequences, and depth cameras, before applying AC.<sup>63,64</sup> In addition, novel MR hardware has been designed to have a lightweight and low density in order to reduce photons attenuation within PET imaging.<sup>65,66</sup>

### **Strategies for Dealing with Body Truncation**

Oncological PET/MR imaging suffers from inhomogeneity of the magnetic field and nonlinearity of the gradient field which leads to geometric distortion and truncation in the transverse plane (patients' arms are normally truncated), considering that the MR FOV is smaller than the typical 60 cm PET FOV. This geometric distortion or body truncation would be reflected in MRI-derived AC maps, wherein MLAA algorithms were suggested to predict the missing areas in the resulting PET AC maps. The other approach to address the truncation issue (employed in clinical routine) is magnetic field harmonization based on gradient enhancement (HUGE), which compensates for the gradient and magnetic field inhomogeneities through optimizing readouts for each arm and the entire slices at the margin of the MR FOV.<sup>67</sup> In addition, deep learning approaches have enabled the completion of the truncated MR-derived AC maps relying only on the truncated MR images,<sup>68</sup> or applying direct attenuation and scatter correction in the image domain.<sup>69</sup> Representative PET images reconstructed using HUGE plus Dixon and Dixon plus MLAA are shown in Fig. 5.

### **Metal Artefact Reduction Techniques**

Due to the susceptibility of MR magnetic fields to metallic objects, the presence of dental fillings, endoprostheses, and surgical devices would result in voids and/or distorted areas in MR images which would adversely impact the MRI-derived PET AC maps, and consequently PET quantification and lesion detectability.<sup>70,71</sup> To address the issue of metallic artifacts in PET/MRI imaging, dedicated MR sequences have been developed to show no or less susceptibility to metal implants. This includes the MAVRIC sequence, which works on the basis of multispectral 3D data acquisition with low sensitivity to metal implants.<sup>71</sup> However, due to the very long acquisition time, its clinical application for MRI-guided AC was not practically feasible.<sup>72</sup> MLAA algorithms are alternative approaches to estimate and/or correct PET AC maps from raw PET data.<sup>73</sup> Atlas-based AC map generation and inpainting methods are also capable of diminishing the adverse impact of metal artifacts in PET AC maps.<sup>51</sup> Similar to body truncation, deep learning approaches could be employed to compensate for metal artifacts in the PET AC map,<sup>68</sup> or directly apply attenuation and scatter correction in the image domain to avoid the negative impact of metal artifacts.<sup>74</sup> Nevertheless, none of the proposed metal artifact reduction methods have provided reliable and

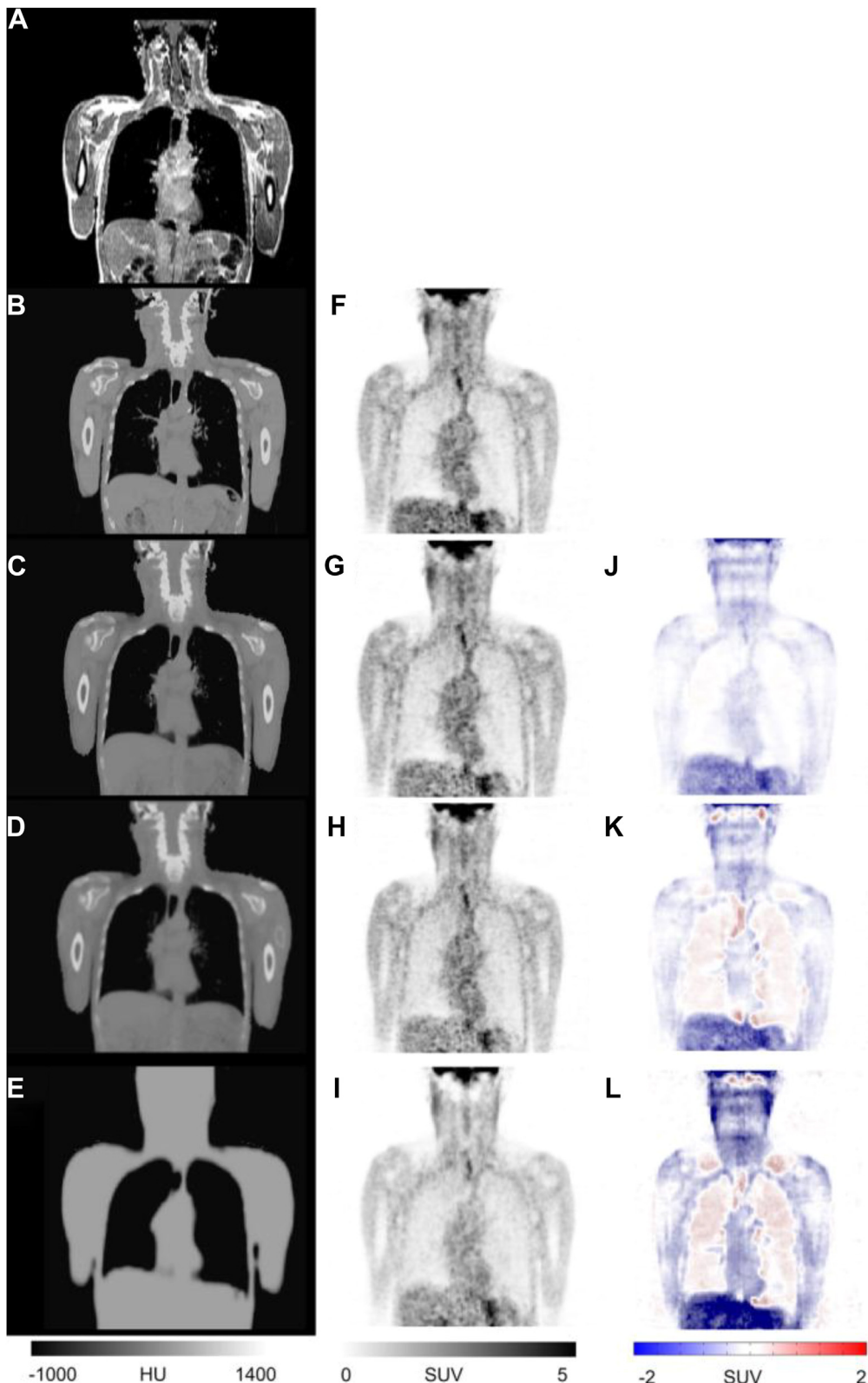


**Fig. 4.** Representative synthetic or pseudo-CT images generated by segmentation-based, atlas-based, and deep learning-based methods along with the corresponding PET images and the bias maps with respect to the reference CT-based PET AC. (A) MR images, (B) Reference CT, (C) Deep learning-based AC map, (D) Atlas-based AC map, (E) Segmentation-based AC map, (F) PET-CT, (G) PET-deep, (H) PET-atlas, (I) PET-segmentation, and (J), (K), and (L) shows their corresponding bias map with respect to the reference PET-CT, respectively. (Reprinted under a Creative Commons License.<sup>51</sup>)

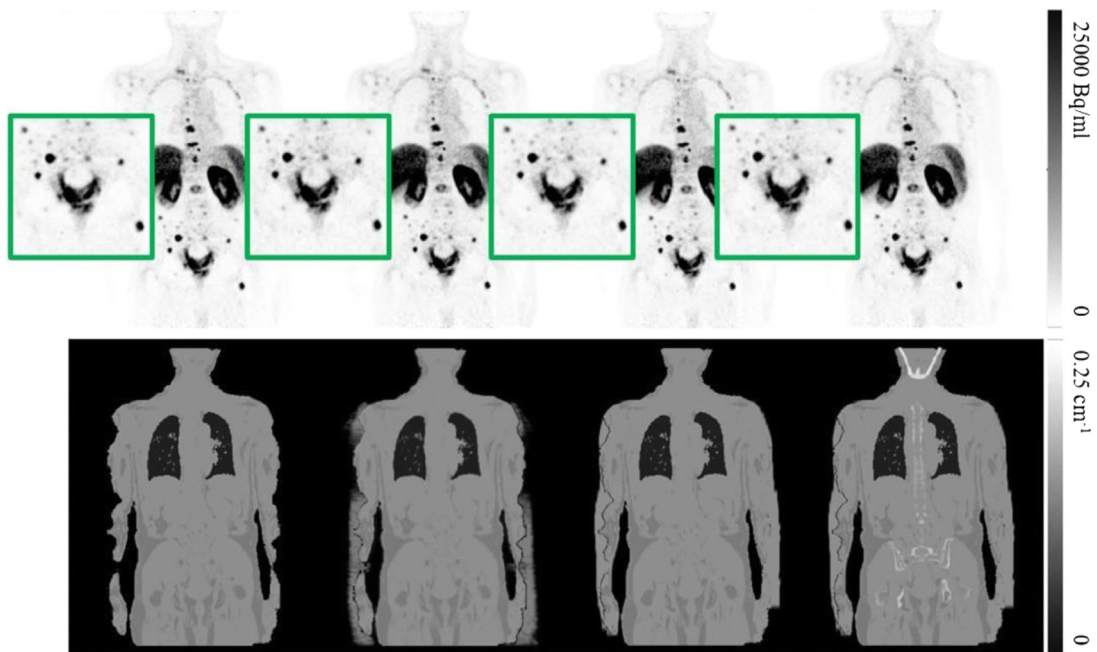


**Fig. 5.** (Top row)  $^{18}\text{F}$ -PSMA PET images reconstructed with four different AC approaches, (Bottom row) corresponding AC maps obtained from standard Dixon, MLAA with Dixon prior, HUGE with Dixon, HUGE with Dixon, and bones. (Reprinted under a Creative Commons License from Springer Nature.<sup>50</sup>)

robust image reconstruction in the context of clinical PET/MR imaging, and as such, this issue warrants further investigation.<sup>3</sup>

#### MAGNETIC RESONANCE IMAGING-GUIDED MOTION CORRECTION IN POSITRON EMISSION TOMOGRAPHY/MAGNETIC RESONANCE IMAGING

Patient motion during PET imaging is a major source of image quality degradation leading to blurred structures, misalignment between PET and MR images (or AC map), and quantification errors.<sup>75</sup> An advantage of simultaneous PET/MR imaging (compared to PET/CT) could be the capability of MR imaging to provide the required information for motion correction, wherein cardiac, respiratory, and gross patient motions could be detected by MR sequences. Cardiac PET/MR imaging, in contrast to PET/CT, requires longer acquisition time and thus is more susceptible to patient and internal organ movements, wherein a mean misalignment error of  $7 \pm 4$  mm between PET and AC images was observed in 90% of the subjects.<sup>76</sup> To avoid gross motion errors, strict quality control of MRI-guided AC is required in cardiac PET imaging, where multiple AC sequences could be acquired (no issues with radiation dose) to select the most appropriate one for PET AC. MRI-guided motion estimation is an efficient approach for artifact-

free PET AC owing to the absence of exposure to ionizing radiation, wherein fast MR sequences, such as 3D multi-echo could be triggered several times by control devices such as EEG electrodes or respiratory belts.<sup>77</sup> MR sequences that allow for the direct estimation of motion vectors in MR space are attractive options for AC of PET data and have shown promising results in FDG PET/MR cardiac imaging.<sup>78,79</sup> A disadvantage of these approaches would be the time needed for dedicated MR sequences and the navigation capabilities within PET imaging which may confine diagnostic MR imaging.

Respiratory motion correction could be conducted using only the emission data; however, since these methods rely on regions with high uptake to estimate the underlying motion vectors, they are not applicable to radiotracers with low target tracer uptake.<sup>80</sup> MLAA algorithms and deep learning-based AC solutions could address the issue of emission and AC image mismatches. However, they are not capable of correcting the emission data for patient or internal organ movements within PET imaging. In this regard, MRI-guided approaches with the capability of providing real-time motion assessment would be the optimal solution for applying motion correction to PET data as well as corresponding AC maps.

In brain PET imaging, due to head bulk motion, motion-corrected image reconstruction (MCIR)

could be conducted, wherein motion information is extracted from MR imaging (magnetization-prepared rapid gradient echo) within PET acquisition (gated PET image reconstructions are transformed to a common gate a posteriori).<sup>81</sup> An example of MRI-guided PET motion correction is presented in Fig. 6.

Deep learning approaches have been successfully applied to estimate motion information from navigator MR sequences (using generative adversarial neural networks), where improved quantitative accuracy, as well as superior visualization quality, was reported compared to the reconstruct-transform average approach.<sup>8,82,83</sup> Radial schemes of MRI acquisitions were employed to estimate and model organ motion in abdominal PET/MR imaging and conducting PET and MR MCIR. Using this strategy, both PET and structural MR images will be corrected for internal organ motion (sharper organ boundaries), thus offering improved diagnostic accuracy.<sup>84</sup>

#### MAGNETIC RESONANCE IMAGING-GUIDED PARTIAL VOLUME CORRECTION IN HYBRID POSITRON EMISSION TOMOGRAPHY/MAGNETIC RESONANCE IMAGING

A distinct advantage of simultaneous PET/MR imaging is the possibility of using prior knowledge extracted from MR images to enhance the quality of PET image reconstructions (MRI-guided PET reconstruction).<sup>85</sup> Statistical priors, extracted from the anatomic MRI data, could be employed within PET image reconstruction (modeled in the system matrix) to improve image reconstruction convergence, suppress noise, enhance the quantitative accuracy, and perform partial volume correction.<sup>86,87</sup>

Partial volume correction (PVC), which leads to enhanced quantitative accuracy as well as improved visual quality of PET images, could greatly benefit from high-contrast structural MR images perfectly aligned to the PET signals in simultaneous PET/MR imaging.<sup>87</sup> PVC approaches relying solely on MR signals to perform PVC, would cause factitious signals in case of mismatches between emission and structural information.<sup>88</sup> Moreover, these approaches tend to suppress signals present only in PET images with no counter structure in MR images. To address this issue, synergistic PET and multiparametric MR priors are employed to diminish the sensitivity to signal mismatches between PET and MRI data and preserve the unique structures in PET images, such as lesions with no equivalent edges/signals on MR images.<sup>85</sup> Nevertheless, these approaches may show high sensitivity to the high noise levels in PET images since strong noise signals would be regarded as genuine structures.<sup>10</sup>

To match the resolutions of PET and MR images, MR images are commonly down-sampled to PET images since increased noise levels and Gibbs artifacts are observed when PET data are upsampled. In this regard, a smooth Lange prior was considered in MRI-guided PET image reconstruction (maximum a posteriori) to perform PVC at a high spatial resolution on PET images.<sup>87</sup>

Recently, deep learning solutions have been proposed to apply post-reconstruction PVC either with or without using MRI support.<sup>89,90</sup> The aim of these approaches was to apply fast PVC without the need for co-registered structural MR information. An example of this approach is presented in Fig. 7. The bulk of research in MRI-guided PET image reconstruction and post-reconstruction PVC

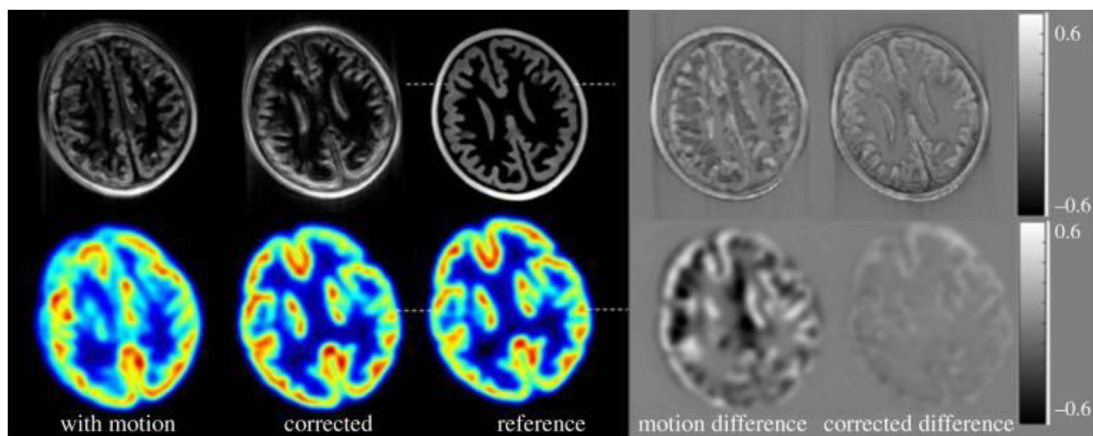


**Fig. 6.** MRI-guided PET motion correction. MR and PET images before and after motion correction are presented together with the difference maps before and after motion correction. (P M Johnson et al 2019. Rigid-body motion correction in hybrid PET/MRI using spherical navigator echoes, Physics in Medicine & Biology, 64 (8), NT03. DOI 10.1088/1361-6560/ab10b2.<sup>83</sup>)

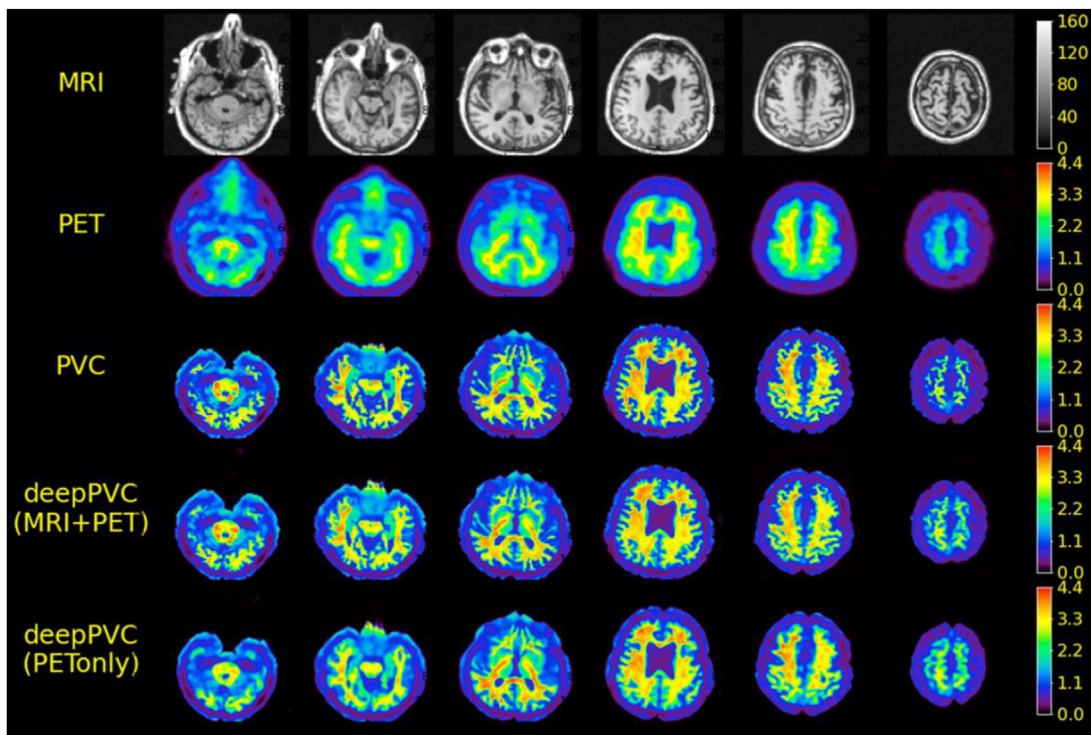


**Fig. 7.** Deep learning-based partial volume correction of PET data with and without using anatomic MRI information. (Reprinted with permission from Springer Nature.<sup>90</sup>)

has been conducted in brain PET/MR imaging, which is less vulnerable to misalignment errors. The feasibility of MRI-guided PET PVC in other body regions and whole-body imaging warrants further research and development efforts.<sup>91</sup>

## SUMMARY AND FUTURE PERSPECTIVES

Over a decade has passed since the introduction of hybrid PET/MRI scanners into clinical practice and yet this technology has yet to found its niche in clinical setting. This could be attributed to the lack of key applications or irreplaceable features of this modality compared to hybrid PET/CT imaging, rather than its technical challenges/limitations, including attenuation correction for PET data. Owing to the continuous advances in detectors and electronic readouts, the trend is toward developing compact PET inserts for existing MRI scanners providing high spatial resolution and reasonable cost. This technology is attracting much attention in research environment owing to the fact that simultaneous PET/MRI imaging would enable accurate motion correction of PET data, partial volume correction, MRI-assisted PET image reconstruction or low-dose PET imaging, and MRI-based cardiac or respiratory gated imaging.

Owing to the extraordinary performance of artificial intelligence or deep learning approaches, algorithms belonging to this category are predominately employed to address the major challenges in PET/MR imaging, such as AC synthetic CT estimation from MR images, body truncation, attenuation and scatter correction of PET data, noise and metal artifact reduction.

## DISCLOSURE

The authors have no potential conflicts of interest to disclose.

## ACKNOWLEDGMENTS

This work was supported by the Swiss National Science Foundation under grant SNF 3200030\_176052 and the Private Foundation of Geneva University Hospitals under grant RC-06 to 01.

## REFERENCES

1. Zaidi H, Del Guerra A. An outlook on future design of hybrid PET/MRI systems. *Med Phys* 2011;38(10): 5667–89.
2. Zaidi H, Becker M. The Promise of hybrid PET/MRI: Technical advances and clinical applications. *IEEE Sign Proc Mag* 2016;33(3):67–85.

3. Bogdanovic B, Solari EL, Villagran Asires A, et al. PET/MR Technology: Advancement and Challenges. *Semin Nucl Med* 2022;52(3):340–55.
4. Currie GM, Leon JL, Nevo E, et al. PET/MR Part 4: Clinical Applications of PET/MRI. *J Nucl Med Technol* 2021. <https://doi.org/10.2967/jnmt.121.263288>.
5. Torigian DA, Zaidi H, Kwee TC, et al. PET/MR Imaging: Technical aspects and potential clinical applications. *Radiology* 2013;267(1):26–44.
6. Mannheim JG, Schmid AM, Schwenck J, et al. PET/MRI Hybrid Systems. *Semin Nucl Med* 2018;48(4):332–47.
7. Becker M, Zaidi H. Imaging in head and neck squamous cell carcinoma: the potential role of PET/MRI. *Br J Radiol* 2014;87(1036):20130677.
8. Chen S, Fraum TJ, Eldeniz C, et al. MR-assisted PET respiratory motion correction using deep-learning based short-scan motion fields. *Magn Reson Med* 2022;88(2):676–90.
9. Meng X, Liu H, Li H, et al. Evaluating the impact of different positron emitters on the performance of a clinical PET/MR system. *Med Phys* 2022;49(4):2642–51.
10. Bland J, Mehranian A, Belzunce MA, et al. Intercomparison of MR-informed PET image reconstruction methods. *Med Phys* 2019;46(11):5055–74.
11. Gao Y, Zhu Y, Bilgel M, et al. Voxel-based partial volume correction of PET images via subtle MRI guided non-local means regularization. *Phys Med* 2021;89:129–39.
12. Afaq A, Faul D, Chebrolu VV, et al. Pitfalls on PET/MRI. *Semin Nucl Med* 2021;51(5):529–39.
13. Herzog H, Lerche C. Advances in clinical PET/MRI instrumentation. *Pet Clin* 2016;11(2):95–103.
14. Catana C, Wu Y, Judenhofer MS, et al. Simultaneous acquisition of multislice PET and MR images: initial results with a MR-compatible PET scanner. *J Nucl Med* 2006;47(12):1968–76.
15. Judenhofer MS, Catana C, Swann BK, et al. PET/MR images acquired with a compact MR-compatible PET detector in a 7-T magnet. *Radiology* 2007;244(3):807–14.
16. Schmand M, Burbar Z, Corbeil J, et al. BrainPET: First human tomograph for simultaneous (functional) PET and MR imaging. *Soc Nuclear Med* 2007;45.
17. Kolb A, Wehrl HF, Hofmann M, et al. Technical performance evaluation of a human brain PET/MRI system. *Eur Radiol* 2012;22(8):1776–88.
18. Zaidi H, Ojha N, Morich M, et al. Design and performance evaluation of a whole-body Ingenuity TF PET-MRI system. *Phys Med Biol* 2011;56(10):3091–106.
19. Kalemis A, Delattre BM, Heinzer S. Sequential whole-body PET/MR scanner: concept, clinical use, and optimisation after two years in the clinic. The manufacturer's perspective. *Magma* 2013;26(1):5–23.
20. Delso G, Fürst S, Jakoby B, et al. Performance measurements of the Siemens mMR integrated whole-body PET/MR scanner. *J Nucl Med* 2011;52(12):1914–22.
21. Aklan B, Paulus DH, Wenkel E, et al. Toward simultaneous PET/MR breast imaging: systematic evaluation and integration of a radiofrequency breast coil. *Med Phys* 2013;40(2):024301.
22. Roncali E, Cherry SR. Application of silicon photomultipliers to positron emission tomography. *Ann Biomed Eng* 2011;39(4):1358–77.
23. Chen S, Gu Y, Yu H, et al. NEMA NU2-2012 performance measurements of the United Imaging uPMR790: an integrated PET/MR system. *Eur J Nucl Med Mol Imaging* 2021;48(6):1726–35.
24. Renker D. Geiger-mode avalanche photodiodes, history, properties and problems. *Nucl Instrum Methods Phys Res* 2006;567(1):48–56.
25. Gundacker S, Heering A. The silicon photomultiplier: fundamentals and applications of a modern solid-state photon detector. *Phys Med Biol* 2020;65(17):17tr01.
26. Lundin A. Barrow Neurological Institute Adds PET Imaging System for Research Activities. *AXIS Imaging News* 2022.
27. CUBRESA NuPET™ System. <https://www.cubre.sa.com/nupet/>. Accessed 2023.
28. Pollard AC, de la Cerda J, Schuler FW, et al. Evaluations of the performances of PET and MRI in a simultaneous PET/MRI instrument for pre-clinical imaging. *EJNMMI physics* 2022;9(1):1–14.
29. Lerche C, Lenz M, Bi W, et al. Design and simulation of a high-resolution and high-sensitivity BrainPET insert for 7T MRI. *Nuklearmedizin-Nucl Med*. 2020;59(02):V96.
30. Gonzalez AJ, Gonzalez-Montoro A, Vidal LF, et al. Initial results of the MINDView PET insert inside the 3T mMR. *IEEE Trans Radiat Plasma Med Sci* 2018;3(3):343–51.
31. Won JY, Park H, Lee S, et al. Development and Initial Results of a Brain PET Insert for Simultaneous 7-Tesla PET/MRI Using an FPGA-Only Signal Digitization Method. *IEEE Trans Med Imaging* 2021;40(6):1579–90.
32. Watanabe M, Kawai-Miyake K, Fushimi Y, et al. Application of a Flexible PET Scanner Combined with 3 T MRI Using Non-local Means Reconstruction: Qualitative and Quantitative Comparison with Whole-Body PET/CT. *Mol Imaging Biol* 2022;24(1):167–76.
33. Del Guerra A, Ahmad S, Avram M, et al. TRIMAGE: A dedicated trimodality (PET/MR/EEG) imaging tool for schizophrenia. *Eur Psychiatry* 2018;50:7–20.
34. Kim KY, Son JW, Kim K, et al. Performance Evaluation of SimPET-X, a PET Insert for Simultaneous Mouse Total-Body PET/MR Imaging. *Mol Imaging Biol* 2021;23(5):703–13.
35. Doss KKM, Mion PE, Kao Y-CJ, et al. Performance evaluation of a PET of 7T bruker micro-PET/MR

- based on NEMA NU 4-2008 standards. *Electronics* 2022;11(14):2194.
36. Miyaoka RS, Lehnert AL. Small animal PET: a review of what we have done and where we are going [published online ahead of print 2020/05/02]. *Phys Med Biol* 2020;65(24).
  37. Bebié P, Becker R, Commichau V, et al. SAFIR-I: Design and Performance of a High-Rate Preclinical PET Insert for MRI. *Sensors* 2021;21(21) [published online ahead of print 2021/11/14].
  38. Emvalomenos G, Trajanovska S, Pham BTT, et al. Performance evaluation of a PET insert for preclinical MRI in stand-alone PET and simultaneous PET-MRI modes. *EJNMMI Phys* 2021;8(1):68.
  39. Mehranian A, Arabi H, Zaidi H. Vision 20/20: Magnetic resonance imaging-guided attenuation correction in PET/MRI: Challenges, solutions, and opportunities. *Med Phys* 2016;43(3):1130–55.
  40. Izquierdo-Garcia D, Catana C. MR Imaging-Guided Attenuation Correction of PET Data in PET/MR Imaging. *Pet Clin* 2016;11(2):129–49.
  41. Allen TJ, Henze Bancroft LC, Kumar M, et al. Gadolinium-based contrast agent attenuation does not impact PET quantification in simultaneous dynamic contrast enhanced breast PET/MR. *Med Phys* 2022;49(8):5206–15.
  42. Martinez-Moller A, Souvatzoglou M, Delso G, et al. Tissue classification as a potential approach for attenuation correction in whole-body PET/MRI: evaluation with PET/CT data. *J Nucl Med* 2009;50(4):520–6.
  43. Beyer T, Lassen ML, Boellaard R, et al. Investigating the state-of-the-art in whole-body MR-based attenuation correction: an intra-individual, inter-system, inventory study on three clinical PET/MR systems. *Magma* 2016;29(1):75–87.
  44. Arabi H, Rager O, Alem A, et al. Clinical assessment of MR-guided 3-class and 4-class attenuation correction in PET/MR. *Mol Imaging Biol* 2015;17(2):264–76.
  45. Andersen FL, Ladefoged CN, Beyer T, et al. Combined PET/MR imaging in neurology: MR-based attenuation correction implies a strong spatial bias when ignoring bone. *Neuroimage* 2014;84:206–16.
  46. Khalife M, Fernandez B, Jaubert O, et al. Subject-specific bone attenuation correction for brain PET/MR: can ZTE-MRI substitute CT scan accurately? *Phys Med Biol* 2017;62(19):7814–32.
  47. Cabello J, Lukas M, Forstier S, et al. MR-based attenuation correction using UTE pulse sequences in dementia patients. *J Nucl Med* 2015;56(3):423–9.
  48. Delso G, Fernandez B, Wiesinger F, et al. Repeatability of ZTE bone maps of the head. *IEEE Trans Radiat Plasma Med Sci* 2017;2(3):244–9.
  49. Arabi H, Zaidi H. Comparison of atlas-based techniques for whole-body bone segmentation. *Med Image Anal* 2017;36:98–112.
  50. Bogdanovic B, Gafita A, Schachoff S, et al. Almost 10 years of PET/MR attenuation correction: the effect on lesion quantification with PSMA: clinical evaluation on 200 prostate cancer patients. *Eur J Nucl Med Mol Imaging* 2021;48(2):543–53.
  51. Arabi H, Zaidi H. MRI-guided attenuation correction in torso PET/MRI: Assessment of segmentation-, atlas-, and deep learning-based approaches in the presence of outliers. *Magn Reson Med* 2022;87(2):686–701.
  52. Mehranian A, Zaidi H, Reader AJ. MR-guided joint reconstruction of activity and attenuation in brain PET-MR. *Neuroimage* 2017;162:276–88.
  53. Fuin N, Pedemonte S, Catalano OA, et al. PET/MRI in the Presence of Metal Implants: Completion of the Attenuation Map from PET Emission Data. *J Nucl Med* 2017;58(5):840–5.
  54. Nuyts J, Bal G, Kehren F, et al. Completion of a truncated attenuation image from the attenuated PET emission data. *IEEE Trans Med Imaging* 2013;32(2):237–46.
  55. Arabi H, Zaidi H. Applications of artificial intelligence and deep learning in molecular imaging and radiotherapy. *Eur J Hybrid Imaging* 2020;4(1):1–23.
  56. Zaidi H, El Naqa I. Quantitative molecular Positron Emission Tomography imaging using advanced deep learning techniques. *Annu Rev Biomed Eng* 2021;23:249–76.
  57. Chen X, Liu C. Deep-learning-based methods of attenuation correction for SPECT and PET. *J Nucl Cardiol* 2022. <https://doi.org/10.1007/s12350-022-03007-3>.
  58. Arabi H, Bortolin K, Ginovart N, et al. Deep learning-guided joint attenuation and scatter correction in multitracer neuroimaging studies. *Hum Brain Mapp* 2020;41(13):3667–79.
  59. Arabi H, Zaidi H. Deep learning-guided estimation of attenuation correction factors from time-of-flight PET emission data. *Med Image Anal* 2020;64:101718.
  60. Hwang D, Kim KY, Kang SK, et al. Improving the Accuracy of Simultaneously Reconstructed Activity and Attenuation Maps Using Deep Learning. *J Nucl Med* 2018;59(10):1624–9.
  61. Dong X, Wang T, Lei Y, et al. Synthetic CT generation from non-attenuation corrected PET images for whole-body PET imaging. *Phys Med Biol* 2019;64(21):215016.
  62. Eldib M, Bini J, Faul DD, et al. Attenuation Correction for Magnetic Resonance Coils in Combined PET/MR Imaging: A Review. *Pet Clin* 2016;11(2):151–60.
  63. Frohwein LJ, Heß M, Schlicher D, et al. PET attenuation correction for flexible MRI surface coils in hybrid PET/MRI using a 3D depth camera. *Phys Med Biol* 2018;63(2):025033.
  64. Aizaz M, Moonen RPM, van der Pol JA, et al. PET/MRI of atherosclerosis. *Cardiovasc Diagn Ther* 2020;10(4):1120–39.

65. Oehmigen M, Lindemann ME, Lanz T, et al. Integrated PET/MR breast cancer imaging: Attenuation correction and implementation of a 16-channel RF coil. *Med Phys* 2016;43(8):4808.
66. Lee YH, Song KH, Yang J, et al. Fabrication and evaluation of bilateral Helmholtz radiofrequency coil for thermo-stable breast image with reduced artifacts. *J Appl Clin Med Phys* 2022;23(1):e13483.
67. Lindemann ME, Gratz M, Blumhagen JO, et al. MR-based truncation correction using an advanced HUGE method to improve attenuation correction in PET/MR imaging of obese patients. *Med Phys* 2022;49(2):865–77.
68. Arabi H, Zaidi H. Truncation compensation and metallic dental implant artefact reduction in PET/MRI attenuation correction using deep learning-based object completion. *Phys Med Biol* 2020;65(19):195002.
69. Liu F, Jang H, Kijowski R, et al. Deep Learning MR Imaging-based Attenuation Correction for PET/MR Imaging. *Radiology* 2018;286(2):676–84.
70. Catana C. Attenuation correction for human PET/MRI studies. *Phys Med Biol* 2020;65(23):23tr02.
71. Schramm G, Ladefoged CN. Metal artifact correction strategies in MRI-based attenuation correction in PET/MRI. *BJR Open* 2019;1(1):20190033.
72. Kudura K, Oblasser T, Ferraro DA, et al. Metal artifact reduction in (68)Ga-PSMA-11 PET/MRI for prostate cancer patients with hip joint replacement using multiacquisition variable-resonance image combination. *Eur J Hybrid Imaging* 2020;4(1):6.
73. Rezaei A, Schramm G, Willekens SMA, et al. A Quantitative Evaluation of Joint Activity and Attenuation Reconstruction in TOF PET/MR Brain Imaging [published online ahead of print 2019/04/14]. *J Nucl Med* 2019;60(11):1649–55.
74. Guo R, Xue S, Hu J, et al. Using domain knowledge for robust and generalizable deep learning-based CT-free PET attenuation and scatter correction [published online ahead of print 2022/10/07]. *Nat Commun* 2022;13(1):5882.
75. Chen Z, Sforazzini F, Baran J, et al. MR-PET head motion correction based on co-registration of multi-contrast MR images. *Hum Brain Mapp* 2021;42(13):4081–91.
76. Lassen ML, Rasul S, Beitzke D, et al. Assessment of attenuation correction for myocardial PET imaging using combined PET/MRI. *J Nucl Cardiol* 2019;26(4):1107–18.
77. Brown R, Kolbitsch C, Delplancke C, et al. Motion estimation and correction for simultaneous PET/MR using SIRF and CIL. *Philos Trans A Math Phys Eng Sci* 2021;379(2204):20200208.
78. Munoz C, Kunze KP, Neji R, et al. Motion-corrected whole-heart PET-MR for the simultaneous visualisation of coronary artery integrity and myocardial viability: an initial clinical validation. *Eur J Nucl Med Mol Imaging* 2018;45(11):1975–86.
79. Einspäanner E, Jochimsen TH, Harries J, et al. Evaluating different methods of MR-based motion correction in simultaneous PET/MR using a head phantom moved by a robotic system. *EJNMMI Phys* 2022;9(1):15.
80. Benz DC, Buechel RR. The winding road towards respiratory motion correction: is this just another dead-end or do we finally get breathing under control? [published online ahead of print 2019/03/08]. *J Nucl Cardiol* 2020;27(6):2231–3.
81. Chen KT, Salcedo S, Chonde DB, et al. MR-assisted PET motion correction in simultaneous PET/MRI studies of dementia subjects. *J Magn Reson Imaging* 2018;48(5):1288–96.
82. Shiyam Sundar LK, Iommi D, Muzik O, et al. Conditional Generative Adversarial Networks Aided Motion Correction of Dynamic (18)F-FDG PET Brain Studies. *J Nucl Med* 2021;62(6):871–9.
83. Polycarpou I, Soultanidis G, Tsoumpas C. Synergistic motion compensation strategies for positron emission tomography when acquired simultaneously with magnetic resonance imaging. *Philos Trans A Math Phys Eng Sci* 2021;379(2204):20200207.
84. Ippoliti M, Lukas M, Brenner W, et al. Respiratory motion correction for enhanced quantification of hepatic lesions in simultaneous PET and DCE-MR imaging. *Phys Med Biol* 2021;66(9).
85. Mehranian A, Belzung MA, Niccolini F, et al. PET image reconstruction using multi-parametric anato-functional priors. *Phys Med Biol* 2017;62(15):5975–6007.
86. Bland J, Mehranian A, Belzung MA, et al. MR-Guided Kernel EM Reconstruction for Reduced Dose PET Imaging. *IEEE Trans Radiat Plasma Med Sci* 2018;2(3):235–43.
87. Belzung MA, Mehranian A, Reader AJ. Enhancement of Partial Volume Correction in MR-Guided PET Image Reconstruction by Using MRI Voxel Sizes. *IEEE Trans Radiat Plasma Med Sci* 2019;3(3):315–26.
88. Nguyen VG, Lee SJ. Incorporating anatomical side information into PET reconstruction using nonlocal regularization. *IEEE Trans Image Process* 2013;22(10):3961–73.
89. Sanaat A, Shooli H, Böhringer AS, et al. A cycle-consistent adversarial network for brain PET partial volume correction without prior anatomical information. *Eur J Nucl Med Mol Imaging* 2023. <https://doi.org/10.1007/s00259-023-06152-0> [published online ahead of print 20230220].
90. Matsubara K, Ibaraki M, Kinoshita T, for the Alzheimer's Disease Neuroimaging I. DeepPVC: prediction of a partial volume-corrected map for brain positron emission tomography studies via a deep convolutional neural network. *EJNMMI Phys* 2022;9(1):50.
91. Alavi A, Werner TJ, Hoilund-Carlsen PF, et al. Correction for partial volume effect is a must, not a luxury, to fully exploit the potential of quantitative PET imaging in clinical oncology. *Mol Imaging Biol* 2018;20(1):1–3.